3rd URSI AT-AP-RASC, Gran Canaria, 29 May – 3 June 2022

A Frequency-Domain Analysis of a Time-Reversal Cavity for Electromagnetic Waves in Transmission Line Networks

Zhaoyang Wang(1), Hamidreza Karami(1)(2), Elias Le Boudec(1), Marcos Rubinstein(3), and Farhad Rachidi(1)
(1) Ecole Polytechnique Fédérale de Lausanne (EPFL), Lausanne, Switzerland
(2) Bu-Ali Sina University, Hamedan, Iran
(3) University of Applied Sciences of Western Switzerland (HES-SO), Yverdon-les-Bains, Switzerland

Abstract

Recently, a closed time-reversal cavity for electromagnetic waves was demonstrated and experimentally realized using a network of transmission lines. This paper presents an analysis in the frequency domain of the wave propagation characteristics that pertain to the time-reversal cavity. The study illustrates, in the frequency domain, that the backward-propagation wave consists of the converging and diverging components, and only the converging wave constitutes a time-reversed counterpart of the forward-propagation wave. Moreover, it is found that the interfering effect of the diverging wave can exist for any of the observation points along the transmission line network. Finally, the analysis demonstrates that an active time-reversal sink remains effective in the frequency domain to overcome the interfering effect.

1 Introduction

A closed time-reversal cavity was considered to be a purely theoretical assumption because of its requirement of an infinite number of observation points [1, 2, 3]. Recently, it was demonstrated that it is possible to realize a time-reversal cavity using a network of transmission lines [4]. The concept was mathematically proven and experimentally validated. More precisely, it was shown in [4] that a transmission line network terminated on matched impedances is an exact one-dimensional time-reversal cavity. Such a system enables the realization of a time-reversal cavity using a limited number of observation points located at the terminals of the network. In the forward-propagation stage, a transient voltage or current source excites the network at an arbitrary location, and the induced responses are measured at the line terminals. By back-injecting the time-reversed measured response at each line terminal, for a given observation point, a time-reversed copy of its forward-propagation voltage or current is produced in the backward-propagation stage [4].

The study presented in [4] explored the time-reversal cavity in the time domain. This paper presents an investigation focused on identifying in the frequency domain the wave propagation characteristics that pertain to the time-reversal cavity in transmission line networks.

2 Frequency-Domain Analysis of a Time-Reversal Cavity in a Transmission Line Network

The frequency-domain analysis follows the consideration of [4], representing the time-reversal cavity with a Y-shaped inhomogeneous transmission line network. As shown in Fig. 1a, a lumped series voltage source is applied to Line #1 at $x_1 = x_s$, injecting a voltage pulse $V_S(j\omega)$. Consequently, its induced voltage responses are measured at the three line terminals as $V_i(j\omega)$ with i being 1, 2, and 3. In the backward-propagation stage, the measured voltages are time reversed through the complex conjugation operation and back-injected into the network from the respective line terminals. The time-reversed counterpart of $V_i(j\omega)$ is denoted by $V_i^*(j\omega)$ with the superscript "$*$" standing for the complex conjugation operator.

The forward- and backward-propagation voltages at an arbitrary location along the network can be formulated analytically. Without loss of generality, $x_1 = x_o$, which is situated along Line #1 between $x_1 = 0$ and $x_1 = x_s$, is considered to be an observation point. The voltages in the two stages (forward and backward) read respectively[1]

$$\begin{aligned} V_{x_o}^{\mathrm{DT}}(j\omega) = &-\frac{1}{2}V_S(j\omega)\cdot e^{-j\beta_1(\omega)\cdot(x_s-x_o)} \\ &+\frac{1}{2}\rho_{L_1}\cdot V_S(j\omega)\cdot e^{-j\beta_1(\omega)\cdot(2L_1-x_s-x_o)} \end{aligned} \tag{1}$$

and

$$\begin{aligned} V_{x_o}^{\mathrm{RT}}(j\omega) = &-\frac{1}{2}V_S^*(j\omega)\cdot e^{+j\beta_1(\omega)\cdot(x_s-x_o)} \\ &+\frac{1}{2}\rho_{L_1}\cdot V_S^*(j\omega)\cdot e^{+j\beta_1(\omega)\cdot(2L_1-x_s-x_o)} \\ &+\frac{1}{2}V_S^*(j\omega)\cdot e^{-j\beta_1(\omega)\cdot(x_s-x_o)} \\ &-\frac{1}{2}\rho_{L_1}\cdot V_S^*(j\omega)\cdot e^{-j\beta_1(\omega)\cdot(2L_1-x_s-x_o)}, \end{aligned} \tag{2}$$

where $\beta_1(\omega)$ is the phase constant of Line #1 and ρ_{L_1} symbolizes the voltage reflection coefficient at the junction $x_1 = L_1$.

[1] "DT" or "RT" in the superscript indicates that the voltage is evaluated in the forward- or backward-propagation stage.

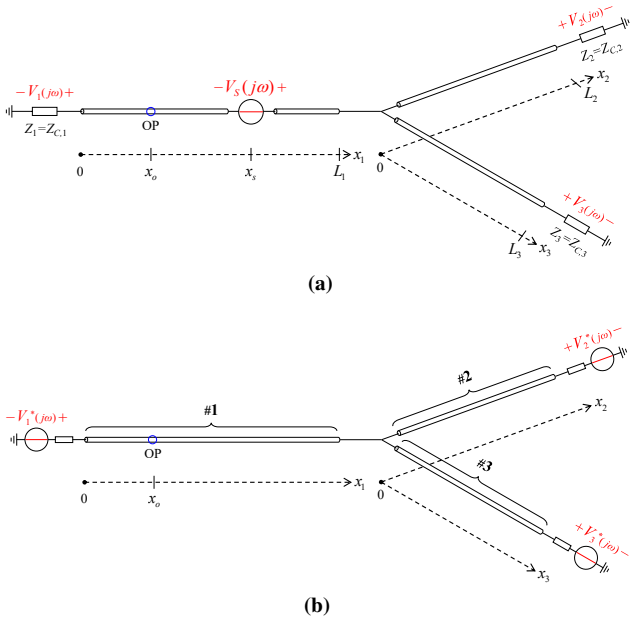

Figure 1. A time-reversal cavity in a Y-shaped transmission line network: (a) forward-propagation stage and (b) backward-propagation stage. $Z_{C,i}$, L_i, and Z_i are, respectively, the characteristic impedance, line length, and terminal impedance of Line #i. The network is terminated with matched impedances, namely $Z_i = Z_{C,i}$. OP indicates an observation point.

Note that, since the transmission line equation is assumed here to satisfy the time-reversal invariance, the derivation of (1) and (2) is based on the lossless line assumption together with the boundary condition of matched-impedance at each line terminal. As a result, ρ_{L_1} is independent of frequency.

According to the expressions (1) and (2), the first two terms of $V_{x_o}^{\mathrm{RT}}(j\omega)$ are the complex conjugate of $V_{x_o}^{\mathrm{DT}}(j\omega)$. That is, the time-domain counterparts of the two terms together behave as a time-reversed function $V_{x_o}^{\mathrm{DT}}(-t)$. In addition, the third and fourth terms of $V_{x_o}^{\mathrm{RT}}(j\omega)$ correspond to an inverted, time-reversed, and time-shifted copy of the first and second terms of $V_{x_o}^{\mathrm{DT}}(j\omega)$ in the time domain, respectively.

These results are in agreement with the time-domain analysis of [4]. Specifically, the first two terms of $V_{x_o}^{\mathrm{RT}}(j\omega)$ are the frequency-domain components of the converging wave present in the backward-propagation stage, and the third and fourth terms represent the diverging wave. Given this fact, we refer to the converging and diverging components as $V_{x_o}^{\mathrm{RT},c}(j\omega)$ and $V_{x_o}^{\mathrm{RT},d}(j\omega)$ hereinafter.

3 Numerical Analysis

This section makes use of a numerical example to analyze the magnitude and phase characteristics of $V_{x_o}^{\mathrm{DT}}(j\omega)$ and $V_{x_o}^{\mathrm{RT}}(j\omega)$ governed by (1) and (2). To this end, the three lines, numbered 1 to 3, of the Y-shaped transmission line network were specified as RG-58, -59, and -179 standard coaxial cables with L_1, L_2, and L_3 being 200 m, 150 m, and 120 m, respectively. A Gaussian-modulated function was employed as the initial excitation whose time- and frequency-domain expressions are given by

$$V_S(t) = e^{-\frac{t^2}{\sigma^2}} \cdot \cos(\omega_0 \cdot t) \tag{3}$$

and

$$V_S(j\omega) = \frac{\sqrt{\pi}}{2}\sigma\left\{e^{-\left[\frac{\sigma}{2}(\omega+\omega_0)\right]^2} + e^{-\left[\frac{\sigma}{2}(\omega-\omega_0)\right]^2}\right\}, \tag{4}$$

where σ is a constant related to the pulse width of $V_S(t)$ and ω_0 determines the center frequency $f_0 = \omega_0/2\pi$ of $V_S(j\omega)$. Note that $V_S(j\omega)$ is real, thus with zero phase angles at all frequencies.

Figure 2 depicts the waveform of $V_S(t)$ and the normalized magnitude curve of $V_S(j\omega)$ in accordance with assigning 28 ns and 40 MHz to σ and f_0, respectively.

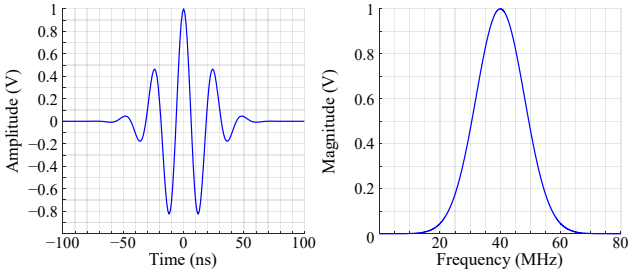

Figure 2. (a) waveform of $V_S(t)$ and (b) normalized magnitude spectrum of $V_S(j\omega)$. The normalization is with respect to the maximum magnitude of $V_S(j\omega)$, namely $|V_S(j\omega_0)|$.

The time-domain study of [4] discussed an interfering effect exerted by the diverging wave. That is, the diverging wave would overlap the converging one if the observation point x_o is located in a region around the source location x_s, satisfying [4]

$$|x_o - x_s| \le \frac{1}{2} v \cdot T_S, \tag{5}$$

where v is the wave propagation speed of the line, along which the source is placed. T_S is the temporal duration of $V_S(t)$. With regard to the case in this text, the interfering region is bounded at $x_1 = x_s \pm 15.8$ m.

Setting $x_s = 80$ m and $x_o = 78$ m, Figs. 3a to 3c present the magnitude spectra of $V_{x_o}^{\mathrm{DT}}(j\omega)$, $V_{x_o}^{\mathrm{RT},c}(j\omega)$, and $V_{x_o}^{\mathrm{RT}}(j\omega)$. For the sake of comparison, the magnitudes over frequencies of each variable are normalized with respect to $|V_S(j\omega_0)|$. In Fig. 3, the envelope lines of the shaded areas represent the normalized magnitudes of the three variables, respectively. The magnitude curve of $V_S(j\omega)$ (shown in Fig. 2b) is also added in each sub-graph of Fig. 3 as a reference.

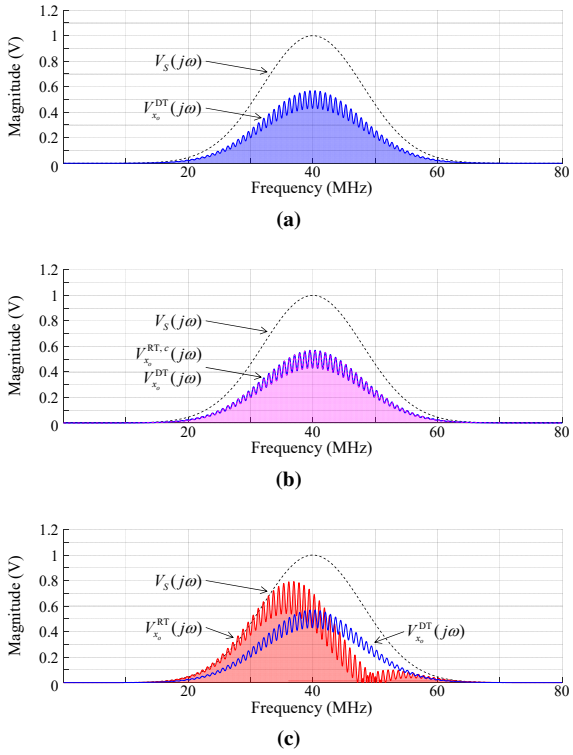

Figure 3. Normalized magnitude spectra of (a) $V_{x_o}^{\mathrm{DT}}(j\omega)$, (b) $V_{x_o}^{\mathrm{RT},c}(j\omega)$, and (c) $V_{x_o}^{\mathrm{RT}}(j\omega)$ for $x_o = 78$ m.

The two envelope lines in Fig. 3b coincide with each other, illustrating the identity between $V_{x_o}^{\mathrm{DT}}(j\omega)$ and $V_{x_o}^{\mathrm{RT},c}(j\omega)$ in terms of the distribution of magnitudes over frequencies. On the other hand, as shown in Fig. 3c, such identity does not hold when comparing the magnitude spectra of $V_{x_o}^{\mathrm{DT}}(j\omega)$ and $V_{x_o}^{\mathrm{RT}}(j\omega)$. The latter incorporates the effect of the diverging component $V_{x_o}^{\mathrm{RT},d}(j\omega)$.

Figure 4 presents a scattering plot in the complex plane, in which $V_{x_o}^{\mathrm{DT}}(j\omega)$, $V_{x_o}^{\mathrm{RT},c}(j\omega)$, and $V_{x_o}^{\mathrm{RT}}(j\omega)$ are normalized and distributed within the region $[-1,1]\times[-j,j]$. It is observed that $V_{x_o}^{\mathrm{DT}}(j\omega)$ and $V_{x_o}^{\mathrm{RT},c}(j\omega)$ are symmetrical with respect to the real axis, while $V_{x_o}^{\mathrm{RT}}(j\omega)$ is merely distributed along the imaginary axis.

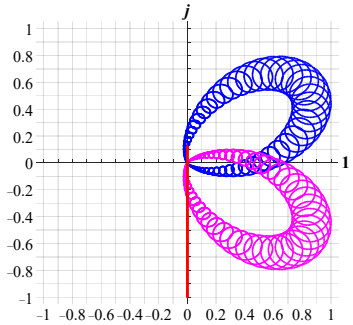

Figure 4. Four-quadrant distribution of the normalized $V_{x_o}^{\mathrm{DT}}(j\omega)$ (in blue), $V_{x_o}^{\mathrm{RT},c}(j\omega)$ (in purple), and $V_{x_o}^{\mathrm{RT}}(j\omega)$ (in red) for $x_o = 78$ m.

To sum up, Figs. 3 and 4 visually explain that, in the backward-propagation stage, only the converging component $V_{x_o}^{\mathrm{RT},c}(j\omega)$ appears to be a time-reversed copy of the forward-propagation voltage $V_{x_o}^{\mathrm{DT}}(j\omega)$. Such a frequency-domain behavior is consistent with the results obtained in the time-domain study [4]. Meanwhile, by assuming an observation point x_o located in the interfering region satisfying the condition (5), it is observed that the diverging component $V_{x_o}^{\mathrm{RT},d}(j\omega)$ interferes with $V_{x_o}^{\mathrm{RT},c}(j\omega)$ in both the magnitude and phase spectra.

Let us now consider an observation point outside the interfering region. Fig. 5 compares the normalized magnitude spectra of $V_{x_o}^{\mathrm{DT}}(j\omega)$ and $V_{x_o}^{\mathrm{RT}}(j\omega)$ for $x_o = 40$ m. As it can be noticed, $V_{x_o}^{\mathrm{RT}}(j\omega)$ differs markedly from $V_{x_o}^{\mathrm{DT}}(j\omega)$ in magnitudes over frequencies. From another perspective, Fig. 6 describes the four-quadrant distribution of the normalized $V_{x_o}^{\mathrm{DT}}(j\omega)$, $V_{x_o}^{\mathrm{RT},c}(j\omega)$, and $V_{x_o}^{\mathrm{RT}}(j\omega)$. For simplicity, only the 1st and 2nd-quadrant components of $V_{x_o}^{\mathrm{DT}}(j\omega)$ are represented. At the corresponding frequency points, $V_{x_o}^{\mathrm{RT},c}(j\omega)$ is symmetrically distributed in the 3rd and 4th quadrants. In contrast, with the addition of the diverging component $V_{x_o}^{\mathrm{RT},d}(j\omega)$, $V_{x_o}^{\mathrm{RT}}(j\omega)$ is located along the imaginary axis.

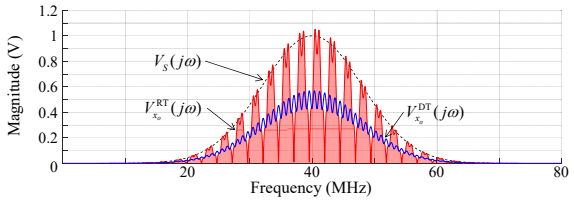

Figure 5. Normalized magnitude spectra of $V_{x_o}^{\mathrm{DT}}(j\omega)$ and $V_{x_o}^{\mathrm{RT}}(j\omega)$ for $x_o = 40$ m.

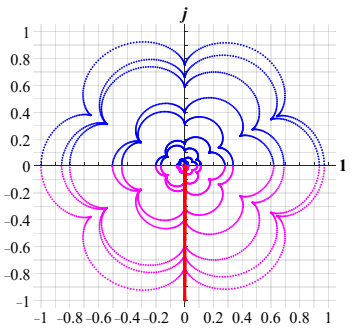

Figure 6. Four-quadrant distribution of the normalized $V_{x_o}^{\mathrm{DT}}(j\omega)$ (in blue), $V_{x_o}^{\mathrm{RT},c}(j\omega)$ (in purple), and $V_{x_o}^{\mathrm{RT}}(j\omega)$ (in red) for $x_o = 40$ m. The plot considers the frequency points where $V_{x_o}^{\mathrm{DT}}(j\omega)$ are distributed in the 1st and 2nd quadrants.

The time-domain analysis of [4] indicates that the diverging wave can be separated completely from the converging wave in time when referring to an observation point located out of the interfering region. However, unlike the time-domain results, $V_{x_o}^{\mathrm{RT},c}(j\omega)$ and $V_{x_o}^{\mathrm{RT},d}(j\omega)$ coexist over

frequencies according to Figs. 5 and 6. Thus, the time-reversed relation between $V_{x_o}^{\mathrm{DT}}(j\omega)$ and $V_{x_o}^{\mathrm{RT},c}(j\omega)$ cannot be straightforwardly inferred in the frequency spectra of $V_{x_o}^{\mathrm{RT}}(j\omega)$ wherever x_o is situated.

Although the interfering effect in the frequency domain is somewhat different from that in the time domain, an active time-reversal sink can remain effective in eliminating the impact of the diverging component $V_{x_o}^{\mathrm{RT},d}(j\omega)$ [4, 5]. Specifically, the original voltage source is assumed to be active at $x_1 = x_s$ in the backward propagation stage and to excite the transmission network with a time-reversed counterpart of the original excitation, namely $V_S^*(j\omega)$. As a result, the induced voltage at $x_1 = x_o$ comprises two terms, which are the third and fourth terms of (2) but with opposite polarity. In this way, the diverging component $V_{x_o}^{\mathrm{RT},d}(j\omega)$ is compensated. More importantly, since only the converging component is present in the backward propagation stage, the foregoing magnitude- and phase-frequency characteristics can be readily observed, confirming that in this case $V_{x_o}^{\mathrm{RT}}(j\omega)$ is a time-reversed counterpart of $V_{x_o}^{\mathrm{DT}}(j\omega)$.

It is also worth noting that the active time-reversal sink is equally applicable to any of the observation points along the transmission line network.

4 Conclusion

We presented a frequency-domain analysis of a time-reversal cavity for electromagnetic waves in transmission line networks. The analysis considered the case of a Y-shaped inhomogeneous transmission line network excited by a lumped series voltage source. Given an observation point located along the network, the voltage acquired in the forward- and backward-propagation stages were formulated analytically using the transmission line equations.

Assuming the observation point to be either within or outside the interfering region (as defined in [4]), the magnitude and phase spectra of the forward and backward voltages were analyzed with reference to a numerical example.

In agreement with the findings of [4], the present study explained in the frequency domain that the backward voltage consists of a converging and a diverging component. It was also confirmed that only the converging component constitutes a time-reversed counterpart of the forward voltage. In addition, it was found that the interfering effect of the diverging component exists regardless of the location of the observation point along the network. Finally, the analysis demonstrated that an active time-reversal sink is effective in the frequency domain to compensate for the effect of the diverging component for any arbitrary observation point.

References

[1] D. Cassereau and M. Fink, "Time-Reversal of Ultrasonic Fields - Part III: Theory of the Closed Time-Reversal Cavity," *IEEE Trans. Ultrason. Ferroelectr. Freq. Control*, vol. 39, no. 5, pp. 579–592, Sep. 1992.

[2] D. Cassereau and M. Fink, "Theoretical Modelisation of Time-Reversal Cavities, Application to Self-Focussing in Inhomogeneous Media," *Acoust. Imaging*, vol. 19, pp. 141–147, 1992.

[3] R. Carminati, R. Pierrat, J. de Rosny, and M. Fink, "Theory of the Time Reversal Cavity for Electromagnetic Fields," *Opt. Lett.*, vol. 32, no. 21, p. 3107, 2007.

[4] Z. Wang, F. Rachidi, M. Paolone, M. Rubinstein, and R. Razzaghi, "A Closed Time-Reversal Cavity for Electromagnetic Waves in Transmission Line Networks," *IEEE Trans. Antennas Propag.*, vol. 69, no. 3, pp. 1621–1630, Mar. 2021.

[5] J. De Rosny and M. Fink, "Overcoming the Diffraction Limit in Wave Physics Using a Time-Reversal Mirror and a Novel Acoustic Sink," *Phys. Rev. Lett.*, vol. 89, no. 12, pp. 124301-1–124301-4, Sep. 2002.